Electronic Supplementary Material (ESI) for Materials Horizons.

Supporting Information

Boron Containing Metal-Organic Framework for Highly Selective Photocatalytic Production of H_2O_2 by Promoting Two-Electron O_2 Reduction

Yujie Li,[a] Fahao Ma,[a] Liren Zheng,[a] Yuanyuan Liu,*[a] Zeyan Wang,[a] Peng Wang,[a] Zhaoke Zheng,[a] Hefeng Cheng,[a] Ying Dai,[b] and Baibiao Huang*[a]

[a]State Key Laboratory of Crystal Materials, Shandong University, Jinan 250100, China.

Email: yyliu@sdu.edu.cn; bbhuang@sdu.edu.cn

[b]School of Physics, Shandong University, Jinan 250100, China.

1. Experimental section

1.1 Materials

Zirconium (IV) chloride ($ZrCl_4$, 98%) was purchased from Alfa Aesar, p-Phthalic acid (PTA, 99%), potassium biphthalate ($C_8H_5KO_4$, 99.8%), methylviologen dichloride ($MVCl_2$), terpineol and potassium iodide (KI, 99%) were purchased from Aladdin Industrial Inc. 4-Carboxyphenylboronic acid (CPBA, 97%) and 1,4-phenylenebisboronic acid (PEBA, 97%) were purchased from Shanghai Macklin Biochemical Co., Ltd. N,N-dimethylformamide (DMF, AR), sodium sulfate anhydrous (Na_2SO_4, AR), benzoquinone (BQ, CP), potassium phosphate monobasic (KH_2PO_4, AR), potassium phosphate dibasic (K_2HPO_4, AR), acetic acid (AR), acetone (AR) and ethanol (AR) were purchased from Sinopharm Chemical Reagent Co., Ltd. All chemicals are commercially available and used without further purification.

1.2 Synthesis of UiO-66

In a typical procedure, $ZrCl_4$ (106 mg, 0.227 mmol) and PTA (76 mg, 0.227 mmol) were dissolved in 52 mL DMF under vigorous stirring for 20 min. Then, 4 mL of acetic acid was added into the solution to modulate the morphology and crystallinity of UiO-66. The mixture was stirred at ambient temperature for 20 min, the obtained homogeneous solution was then transferred into a 100 mL Teflon lined stainless steel autoclave and heated to 150 °C for 60 h. After cooled naturally, the product of the synthesis was washed with DMF followed by acetone to remove unreacted organic linkers, and dried at 60 °C in vacuum oven for 12 h.

1.3 Synthesis of UiO-66-B

The UiO-66-B was prepared according to the same procedure as above, except that the organic ligand is CPBA (76 mg, 0.227 mmol) rather than PTA.

1.4 Synthesis of UiO-66-B-X

The UiO-66-B-X was prepared according to the same procedure as that for UiO-66, except that different content of PTA and CPBA were used as mixed ligand, which were labeled as UiO-66-B-X (X = 20, 40, 60, 80; where X is the molar percentage of CPBA in the organic ligands).

1.5 Characterization

Powder X-ray diffraction (XRD) was performed with a Japan Rigaku SmartLabTM rotation anode X-ray diffractometer (Miniflex 600) equipped with graphite-monochromated Cu Kα radiation (λ= 1.54178 Å). Fourier transform infrared (FT-IR) spectra were obtained on a Bruker Tensor II spectrometer using KBr pellets. The X-ray photoelectron spectroscopy (XPS) was measured on a Thermo Fisher ESCALAB 250XI spectrometer with monochromatized Al Kα excitation. The morphologies of the samples were tested by scanning electron microscope (SEM, Hitachi S-4800). The diffuse reflectance spectroscopy (DRS) of the products were obtained using a UV-2600 Shimadzu UV-Vis spectrophotometer. The steady photoluminescence (PL) spectra and time-resolved photoluminescence (TRPL) decay spectra were measured using a FLS920 fuorescence under 280 nm excitation at room temperature. The specific surface

area, pore-size distribution and pore volume of the samples were measured via a N_2 adsorption–desorption and Brunauer–Emmett–Teller (BET) method by a Micromeritics ASAP Kubo X1000 analyzer at liquid nitrogen temperature. Electron spin resonance (ESR) spectra were recorded with a JEOL JES-RE-2X at room temperature for $\cdot O_2^-$ and liquid nitrogen temperature for Zr^{3+} signal. The O_2 adsorption test were analyzed by Builder PCA-1100 gas adsorption analyzer. The temperature programmed desorption (TPD) of O_2 measurement were obtained by AutoChem II 2920 and 5% O_2-He TCD Calibration, the specimens were equilibrated under 5% O_2 for 1 h after pre-treatment at 300 ºC under He atmosphere for 2 h, followed by an isothermal removal of physically adsorbed O_2 in He for 1 h. TPD measurements were carried out in He at a heating rate of 10 °C/min up to 400 °C. The gas flow rate was 50 mL min^{-1}.

1.6 Photoelectrochemical measurements

Linear sweep voltammetry (LSV), electrochemical impedance spectroscopy (EIS) and transient photocurrent response were performed by a CHI 660D workstation with a three-electrode system in 0.1 M Na_2SO_4. A 300 W Xe lamp was used as the light source. $MVCl_2$ (0.001 M) was added into the electrolyte as a fast electron scavenger to investigate the surface charge transfer efficiency. The catalysts coated on clean FTO glasses acted as working electrodes, while Ag/AgCl and Pt sheet acted as reference and counter electrodes, respectively. The working electrode was prepared as follows: 2 mg photocatalyst was dispersed into the solution containing 300 μL ethanol and 300 μL terpineol under sonication for 20 min to prepare a homogeneous slurry. Then, 200 μL of the slurry was dropped onto the pretreated stannic oxide (FTO) conductive glass with an exposed area of 4.0 cm^2 (2.0 cm × 2.0 cm), then dried to form a film.

The rotating ring-disk electrode (RRDE) measurements were performed on BAS Inc setup with CHI 750E workstation. Ag/AgCl used as a reference and Pt wire as a counter in an electrolyte composed of phosphate buffer (pH = 7, 0.1 M). The RRDE that was composed of a glassy carbon disk and a Pt ring was used as a working electrode. Prior to measurements, the catalyst ink was dropped on the glassy carbon disk and dried at room temperature. The number of the transferred electrons (n) was calculated following equation:

$$x = \frac{4I_d}{I_d + I_r/N}$$

The selectivity of H_2O_2 was determined by equation:

$$H_2O_2\% = 200 \times \frac{I_r/N}{I_d + I_r/N}$$

where I_d is the disc current, I_r is the ring current and N is the collection efficiency. The value of N was experimentally determined to be 0.36 by a standard ferricyanide ($K_3[Fe(CN)_6]$) system.

1.7 The quasi Fermi energy level formula

The carrier density difference between UiO-66 and UiO-66-B in the quasi Fermi level

can be calculated by the formula: $E_{f1} - E_{f2} = kT\ln(N_{f1}/N_{f2})/e$ (where the E_f and N_f are the quasi Fermi level and corresponding carrier density of sample, k is the Boltzmann constant, T is the system temperature during the test and e is elementary charge).

1.8 The photocurrent density formula

The photocurrent density can be described by the formula: $J = J_{max} \times \eta_{abs} \times \eta_{sep} \times \eta_{trans}$. Assuming that the surface charge transfer efficiency in the presence of MV^{2+} is 100%, the photocurrent density can be determined by the formula: $J_{MV} = J_{max} \times \eta_{abs} \times \eta_{sep}$. As shown in Fig. 6f, UiO-66 and UiO-66-B exhibit photocurrent densities at 0.025 and 0.085 μA cm^{-2} in normal electrolyte, while the photocurrent densities increase to 0.141 and 0.249 μA cm^{-2} in the presence of MV^{2+}, respectively. As the J_{max}, η_{abs}, and η_{sep} are unchanged for the J and J_{MV}, the η_{trans} can be calculated by the equation: $\eta_{trans} = J/J_{MV}$.

1.9 Photogeneration of H_2O_2

30 mg of as-synthesized photocatalyst was dispersed into a beaker containing 100 mL isopropanol aqueous solution (10%). The suspension solution was stirred for 30 min in the dark with continually O_2 bubbling to reach the absorption–desorption equilibrium. A 300 W xenon lamp (CEL-HXF300) with an AM-1.5 filter was used as the light source. The light source was located at a distance of 20 cm from the reactor, and continuous magnetic stirring and cooling water (15 °C) were applied during the experiment. During illumination, 3 mL solution was sampled every 20 min and centrifuged to remove the photocatalyst.

The amount of H_2O_2 was analyzed by iodometry. Typically, 1 mL of 0.1 mol L^{-1} potassium phthalate monobasic ($C_8H_5KO_4$) aqueous solution and 1 mL of 0.4 mol L^{-1} potassium iodide (KI) aqueous solution were added to the obtained solution, which stand still for 30 min. The H_2O_2 molecules reacte with iodide anions (I^-) under acidic conditions ($H_2O_2 + 3I^- + 2H^+ \rightarrow I_3^- + 2H_2O$) to produce triiodide anions (I_3^-) possessing a strong absorption at around 350 nm. The amount of I_3^- was determined by measuring the absorption intensity at 350 nm using UV–vis spectra.

1.10 BQ traps superoxide radicals ($\cdot O_2^-$)

It is well accepted that BQ can be used as an $\cdot O_2^-$ scavenger. In order to exclude the effect of BQ on the iodometry, two H_2O_2 solution with the same concentration (400 μmol L^{-1}) were prepared and BQ was added to one solution. After titration and full coloration, the H_2O_2 concentration for the two solution were determined to be the same, i.e. 400 μmol L^{-1}, indicating that the presence of BQ would not affect the iodometry.

1.11 Photocatalytic degradation experiments

To investigate the decomposition behavior of H_2O_2 over prepared photocatalysts, 30 mg of as-prepared photocatalyst was dispersed in 100 mL 3×10^{-3} M H_2O_2 solution, which were irradiated under 300 W xenon lamp with an AM-1.5 filter with continuous stirring. The degradation of H_2O_2 was detected by the same procedure as above.

1.12 Density function theory calculation details

All the density-functional theory (DFT) computations were performed using the Dmol3 software package based on the linear combination of atomic orbitals (LCAO) method. Electron-ion interactions were described using the DFT Semi-core Pseudopots (DSPP)

pseudopotentials. A double numerical polarized (DND) basis set was employed to expand the wave functions with an orbital cutoff of 5.3 Å for Zr, 3.7 Å for C, 3.3 Å for O, 3.1 Å for H and 3.7 Å for B. For the electron-electron exchange and correlation interactions, the functional parametrized by Perdew-Burke-Ernzerhof (PBE), a form of the general gradient approximation (GGA), was used throughout. The vander Waals interaction was described using the DFT-D2 method that proposed by Grimme.

During the geometry optimizations, all the atoms were allowed to relax. In this work, the Brillouin-zone integrations were conducted using Monkhorst-Pack (MP) grids of special points. A k-point sets with a separation of 0.07 $Å^{-1}$ was used for all the model cell. The convergence criterion for the electronic self-consistent field (SCF) loop was set to 10^{-6}. The atomic structures were optimized until the residual forces were below 0.002 Ha $Å^{-1}$.

2. Results

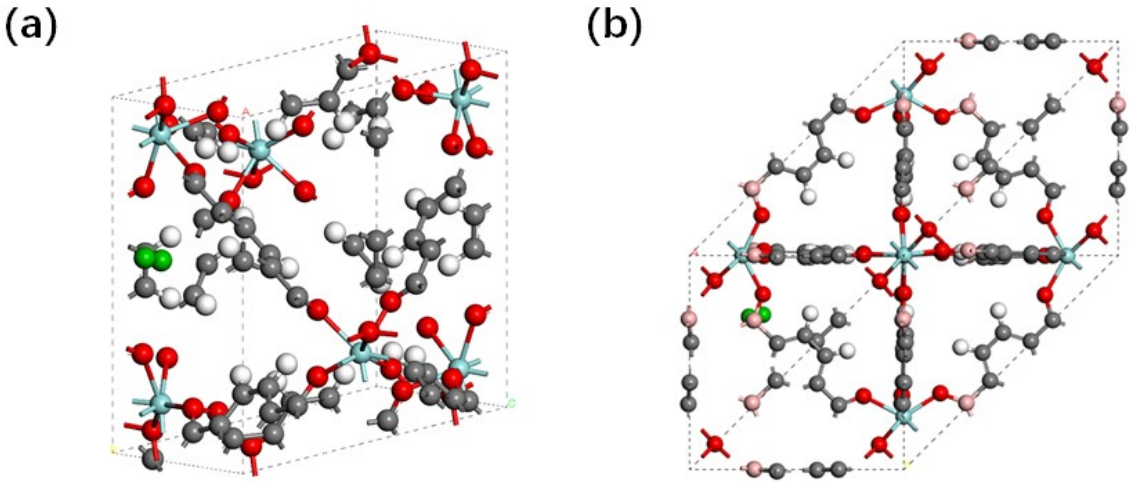

Fig. S1 Optimized structural model of O_2 adsorption by (a) UiO-66 and (b) UiO-66-B (white: H, gray: C, red: O, blue: Zr, green: O_2, pink: B).

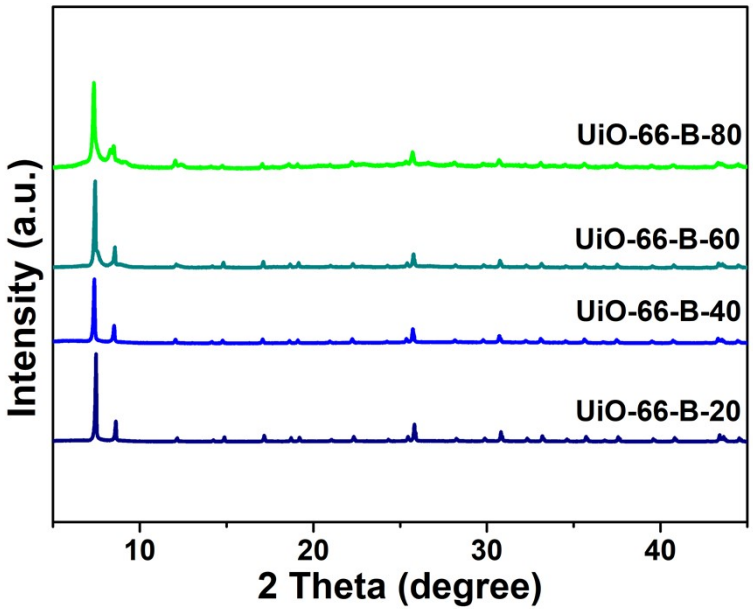

Fig. S2 XRD patterns of UiO-66-B-X (X is the molar percentage of CPBA in the MOF, X=20, 40, 60, 80).

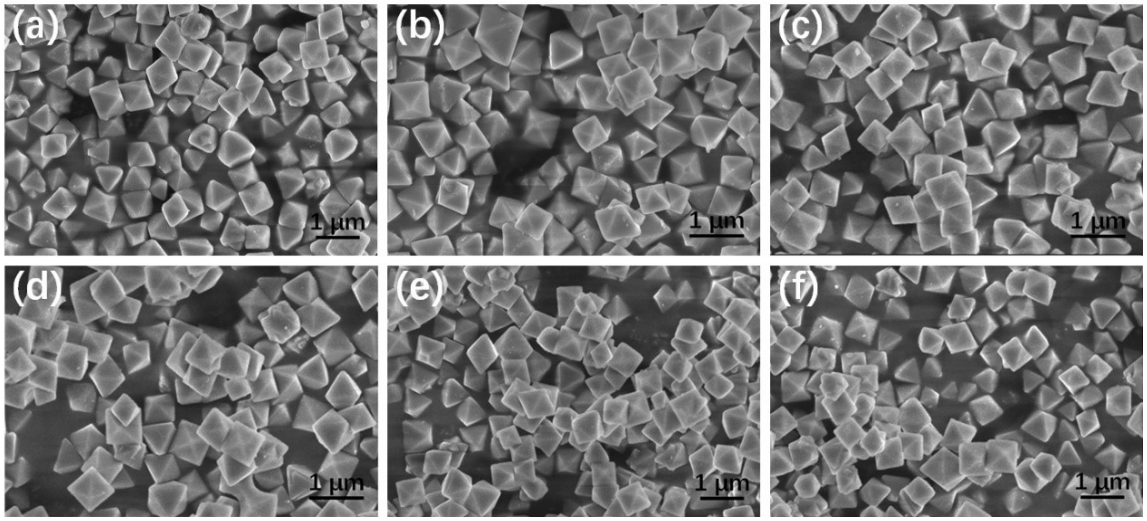

Fig. S3 SEM images of (a) UiO-66, (b) UiO-66-B-20, (c) UiO-66-B-40, (d) UiO-66-B-60, (e) UiO-66-B-80 and (f) UiO-66-B.

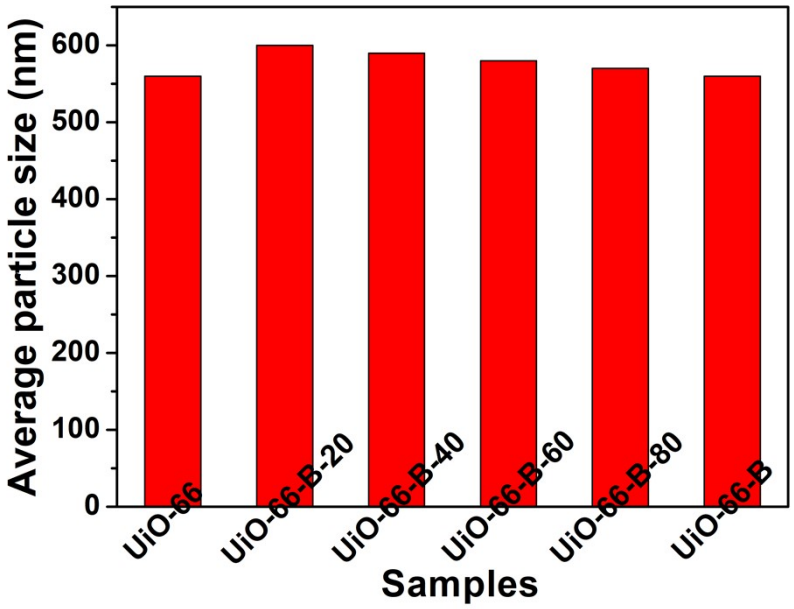

Fig. S4 The average particle size of all the samples mentioned in this work.

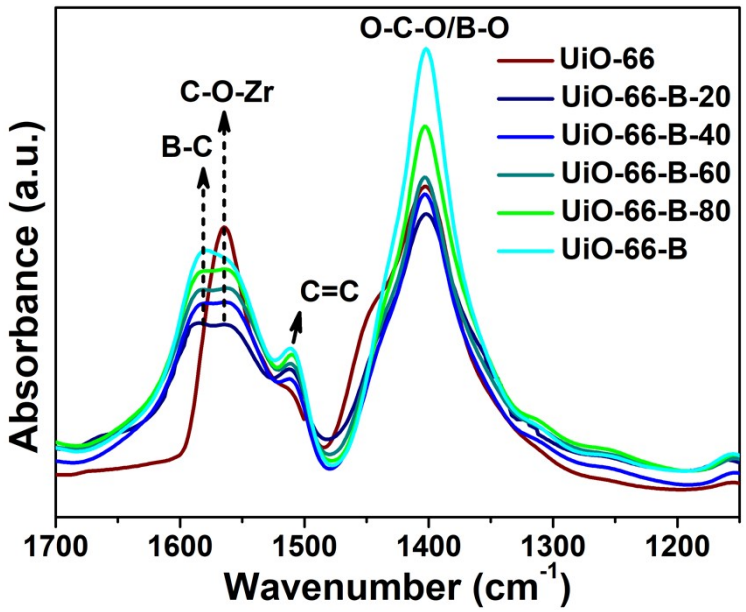

Fig. S5 FT-IR spectra of UiO-66, UiO-66-B-X (X=20, 40, 60, and 80) and UiO-66-B.

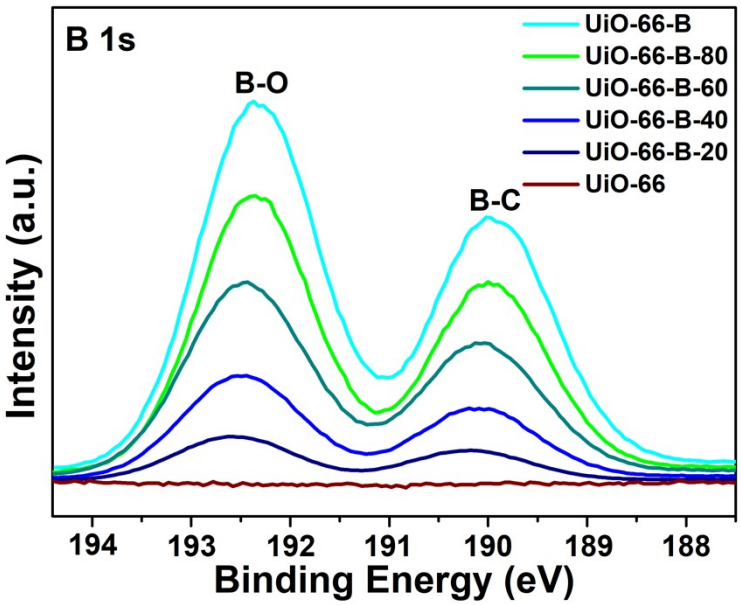

Fig. S6 B 1s high-resolution XPS spectra of UiO-66, UiO-66-B-X (X=20, 40, 60, and 80) and UiO-66-B.

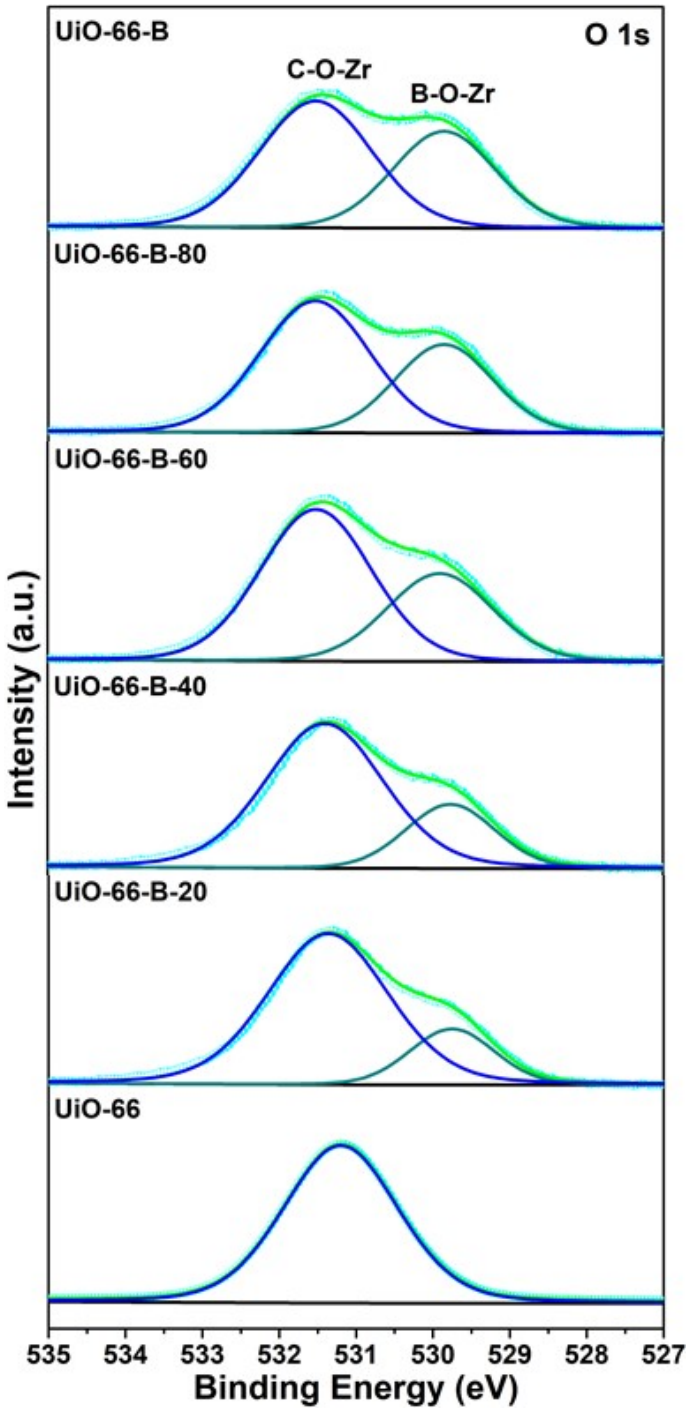

Fig. S7 O 1s high-resolution XPS spectra of UiO-66, UiO-66-B-X (X=20, 40, 60, and 80) and UiO-66-B.

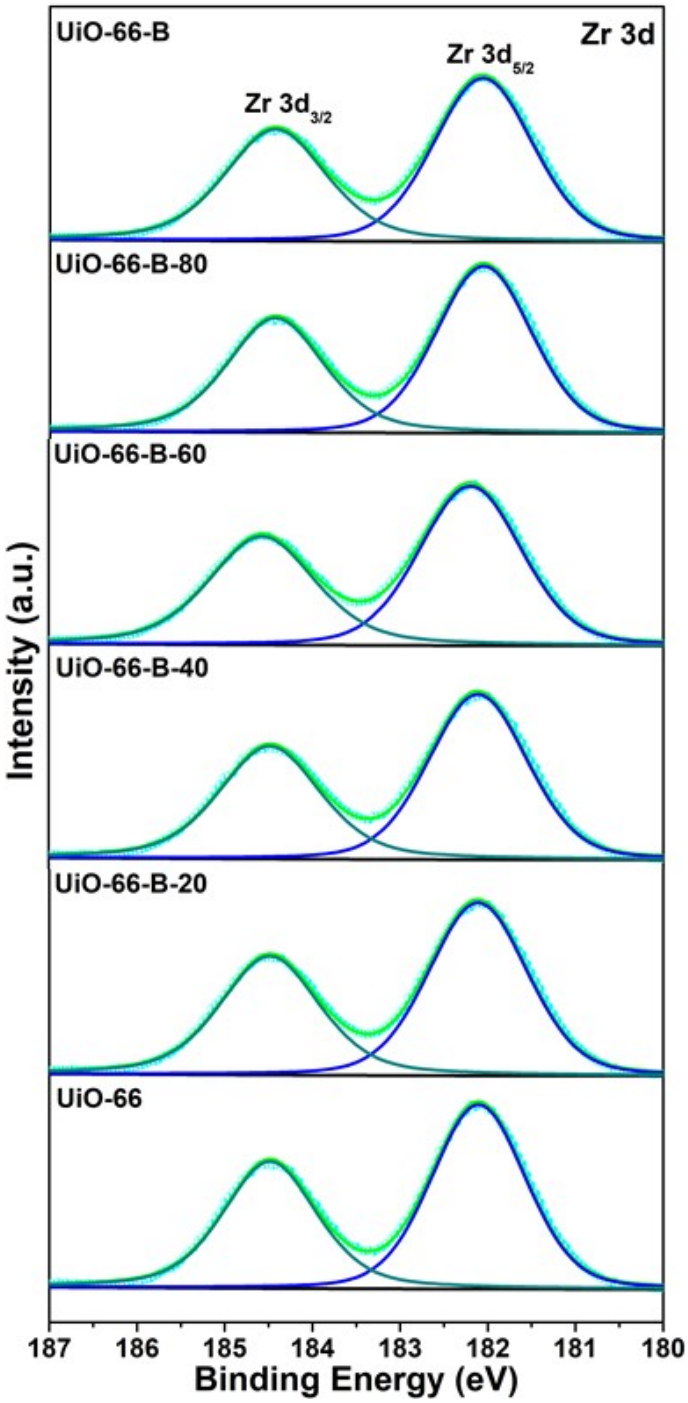

Fig. S8 Zr 3d high-resolution XPS spectra of UiO-66, UiO-66-B-X (X=20, 40, 60, and 80) and UiO-66-B.

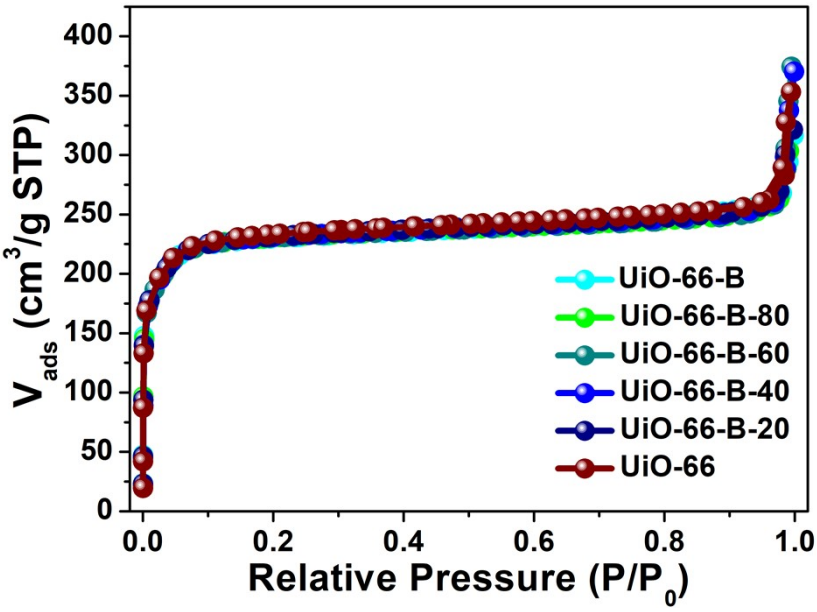

Fig. S9 (a) N_2 adsorption/desorption isotherms at 77 K of UiO-66, UiO-66-B-X (X=20, 40, 60, and 80) and UiO-66-B.

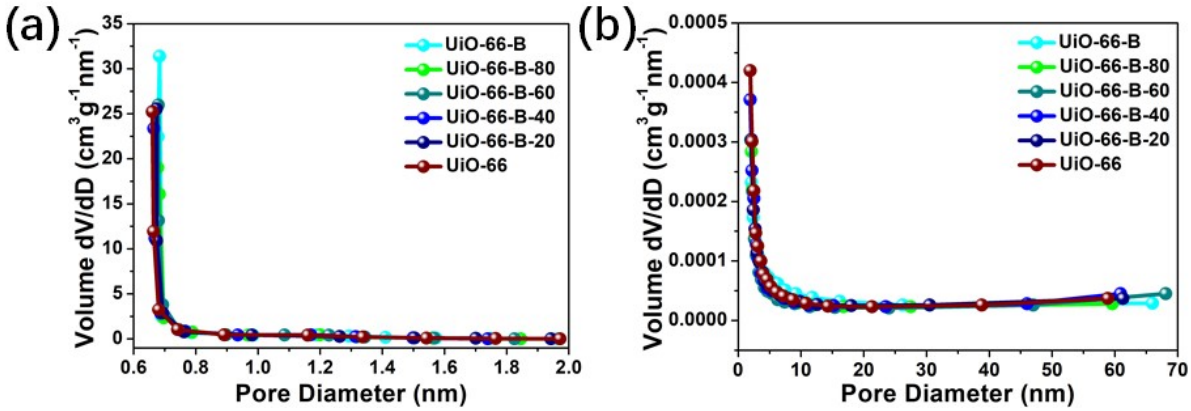

Fig. S10 (a) Horvath-Kawazoe (HK) micropore size distribution and (b) Barrett-Joyner-Halenda (BJH) mesopore size distribution of UiO-66, UiO-66-B-X (X=20, 40, 60, and 80) and UiO-66-B.

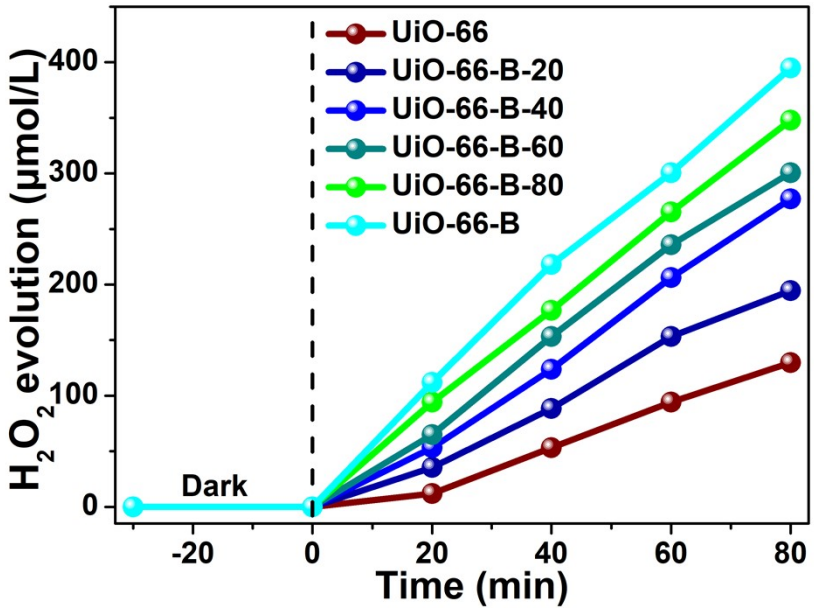

Fig. S11 Time course of H_2O_2 production over UiO-66, UiO-66-B-X (X=20, 40, 60, and 80) and UiO-66-B under simulated sunlight irradiation (reaction conditions: 0.3 g L^{-1} catalyst, 90 mL water + 10 mL isopropanol).

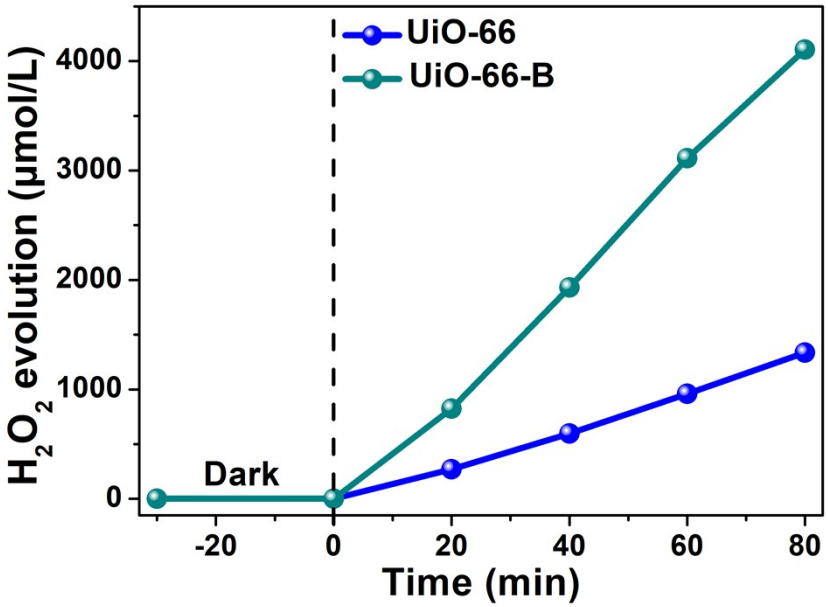

Fig. S12 Time course of H_2O_2 production over UiO-66 and UiO-66-B in isopropanol aqueous solution under UV light irradiation (reaction conditions: 0.3 g L^{-1} catalyst, 90 mL water + 10 mL isopropanol).

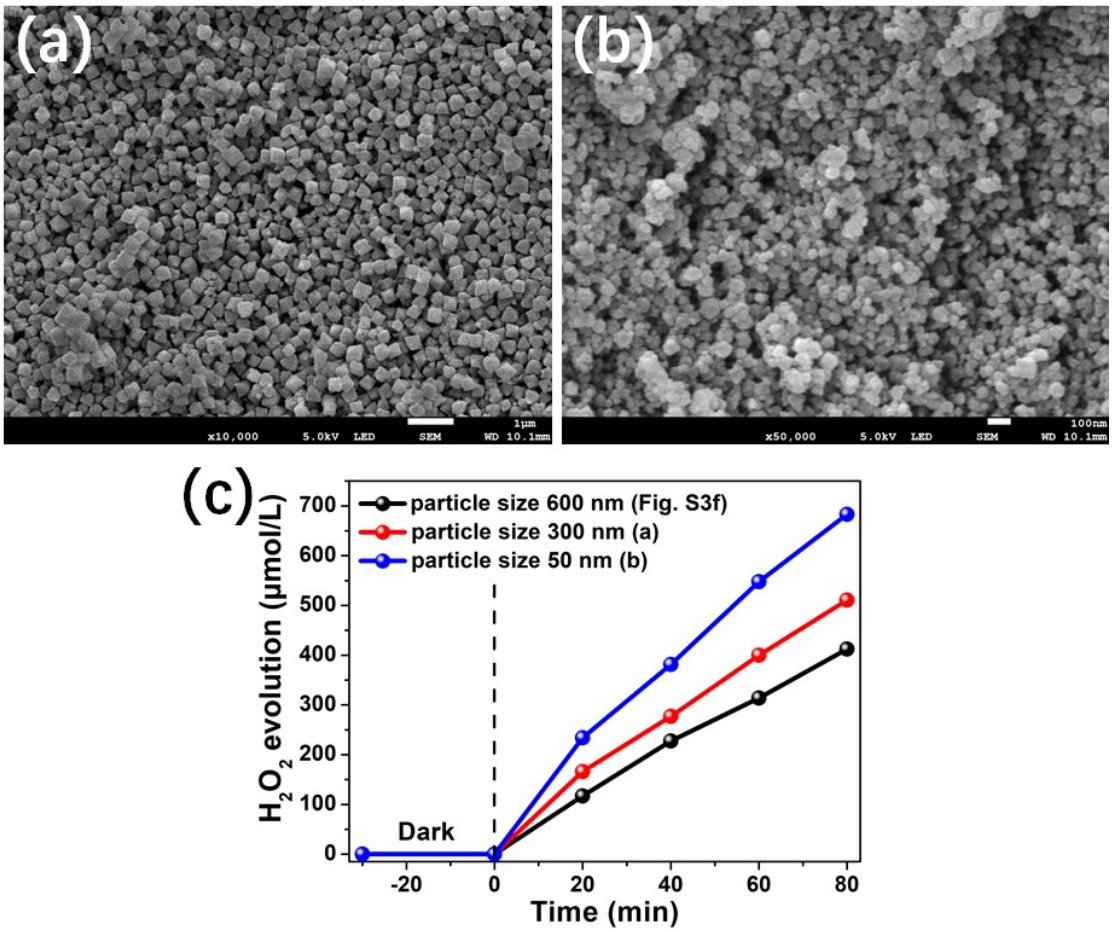

Fig. S13 SEM images of UiO-66-B synthesized in the presence of (a) 30 and (b) 0 equivalents of benzoic acid. (c) Time course of H_2O_2 production over UiO-66-B with different particle sizes under simulated sunlight irradiation (reaction conditions: 0.3 g L^{-1} catalyst, 90 mL water + 10 mL isopropanol).

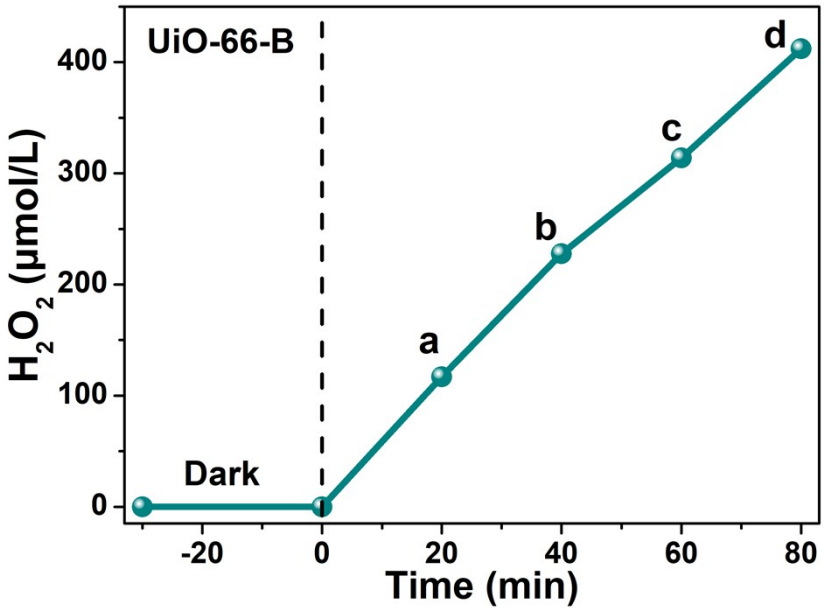

Fig. S14 Time course of H_2O_2 production over UiO-66-B in isopropanol aqueous solution under simulated sunlight irradiation (reaction conditions: 0.3 g L^{-1} catalyst, 90 mL water + 10 mL isopropanol).

The equation $[H_2O_2] = (K_f/K_d)\{1\text{-}\exp(-K_d \times t)\}$ is widely used to determine the rate constant for formation (K_f) and decomposition (K_d) based on the assumption that formation and decomposition follow zero-order and first-order kinetics respectively. For above equation, t is the reaction time, and $[H_2O_2]$ is the concentration of H_2O_2 at time t.

The decoupling is operated as follows:

At time t_a and t_b, the corresponding concentration of H_2O_2 can be determined respectively. Consequently, K_f (7.826 μM min^{-1}) and K_d (0.0160 min^{-1}) can be resolved from equation (1) and (2)

$$[H2O2]_a = (K_f/K_d)\ \{1\text{-}\exp(-K_d \times t_a)\} \quad (1)$$

$$[H2O2]_b = (K_f/K_d)\ \{1\text{-}\exp(-K_d \times t_b)\} \quad (2)$$

In order to obtain more accurate values of K_f and K_d, other points on the curve are also

selected. For example, t_c and t_d can replace t_a and t_b, and another group of K_f (7.822 μM min^{-1}) and K_d (0.0162 min^{-1}) can be obtained.

Finally, average values for K_f (7.824 μM min^{-1}) and K_d (0.0161 min^{-1}) are obtained.

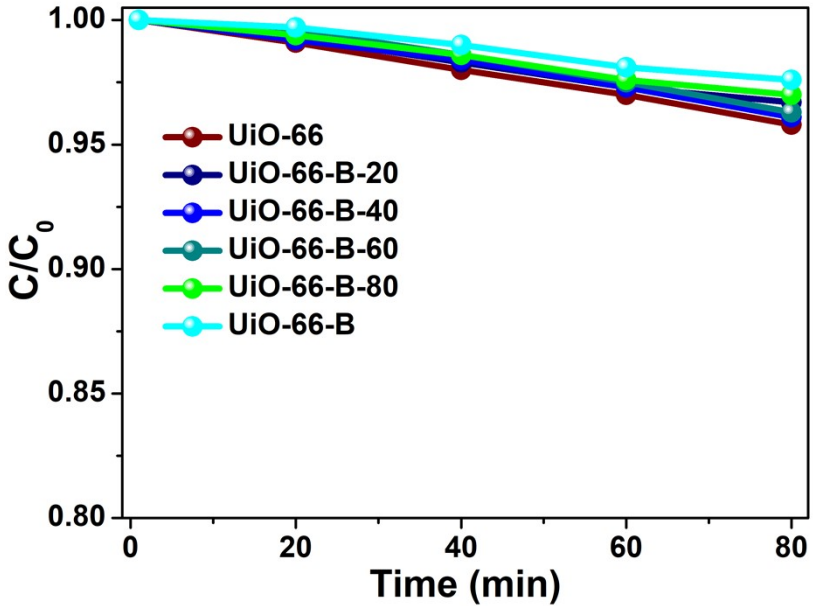

Fig. S15 The photocatalytic decomposition of H_2O_2 over UiO-66, UiO-66-B-20, UiO-66-B-40, UiO-66-B-60, UiO-66-B-80, and UiO-66-B under simulated sunlight (AM 1.5) irradiation (reaction conditions: 0.3 g L^{-1} catalyst, 100 mL water, 3mM H_2O_2).

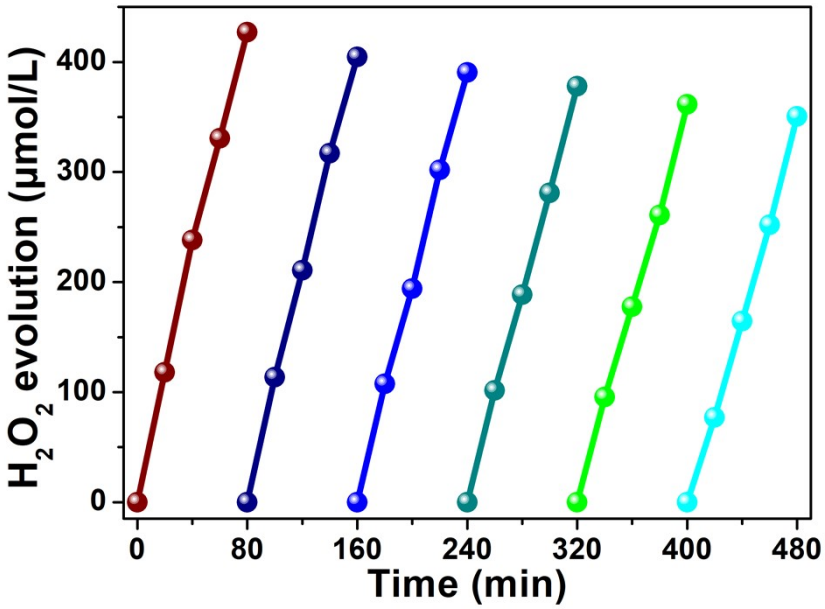

Fig. S16 Cycling runs for the photocatalytic H_2O_2 production over UiO-66-B.

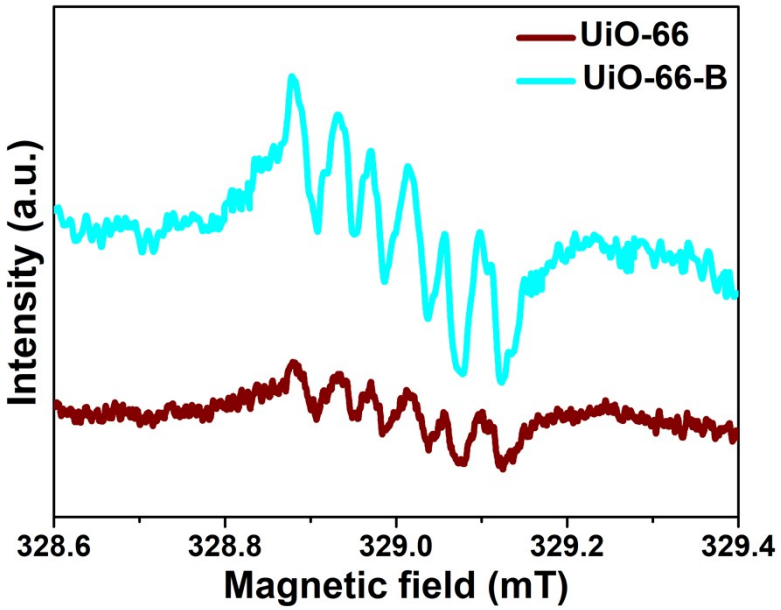

Fig. S17 ESR signals of DMPO-·O_2^- over UiO-66 and UiO-66-B under simulated sunlight irradiation.

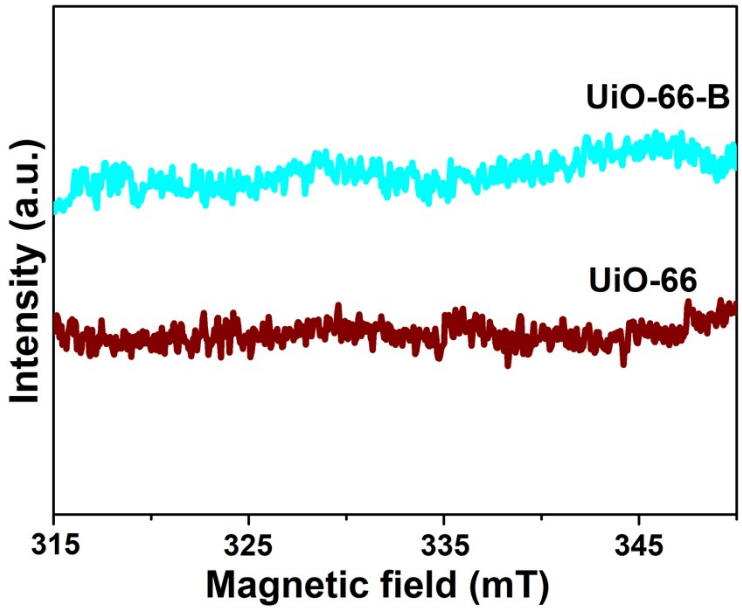

Fig. S18 ESR spectra recorded at 77K of UiO-66 and UiO-66-B in the isopropanol aqueous solution without light irradiation.

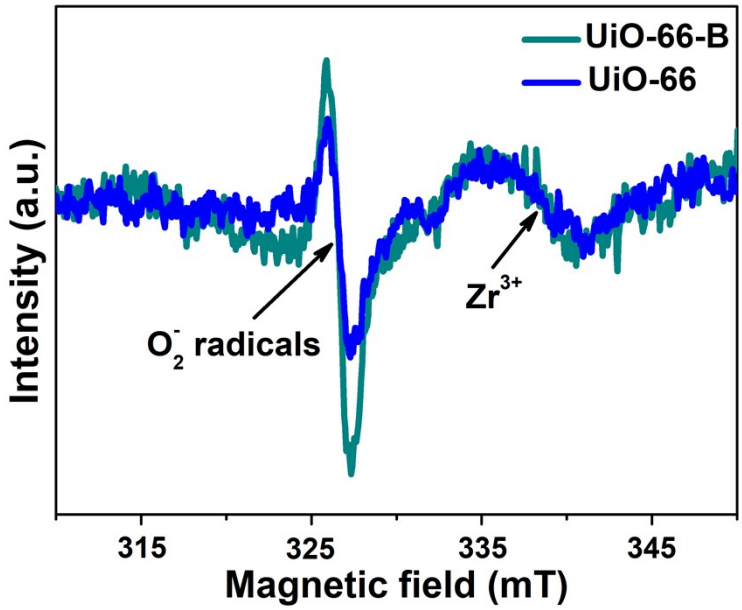

Fig. S19 ESR spectra of UiO-66 and UiO-66-B recorded at 77K under simulated sunlight irradiation in the isopropanol aqueous solution.

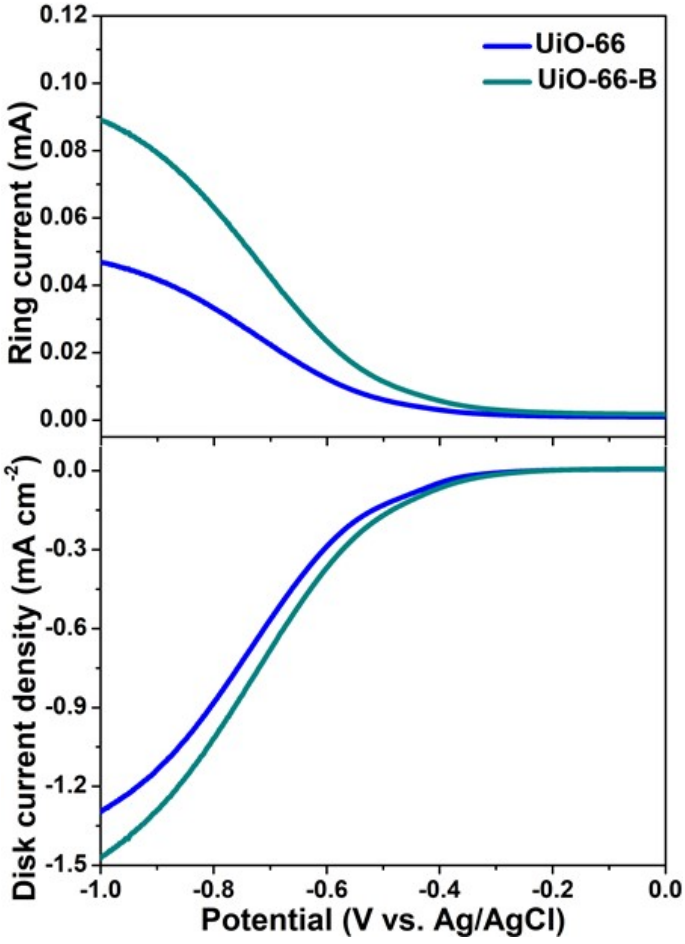

Fig. S20 RRDE polarization curves for the UiO-66 and UiO-66-B-coated electrodes at

1600 rpm in O_2-saturated electrolyte using the ring current (top) and the disc current (bottom).

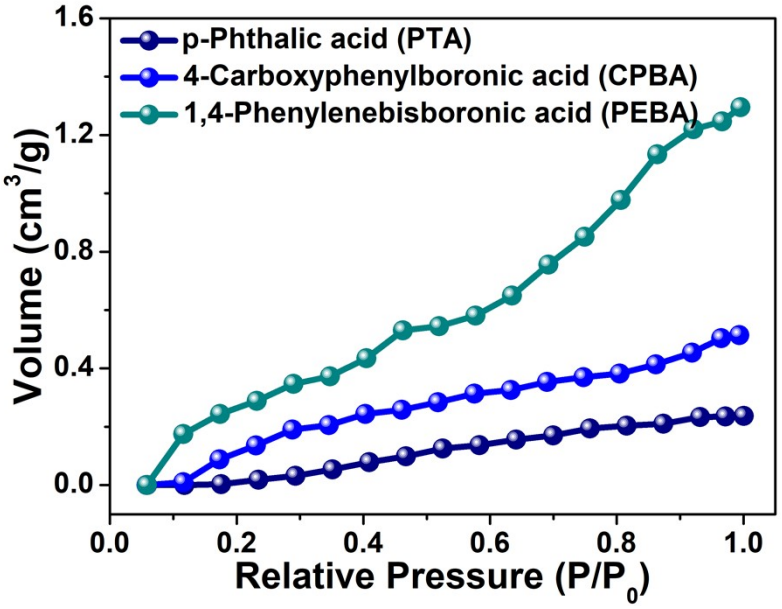

Fig. S21 O_2 adsorption isotherms of PTA, CPBA and PEBA ligands at 298 K.

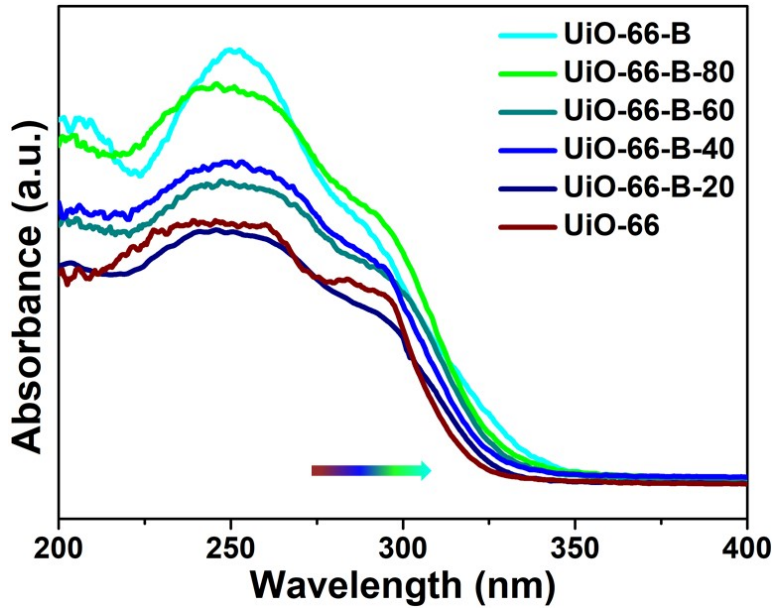

Fig. S22 UV-vis DRS of UiO-66, UiO-66-B-X (X=20, 40, 60, and 80) and UiO-66-B.

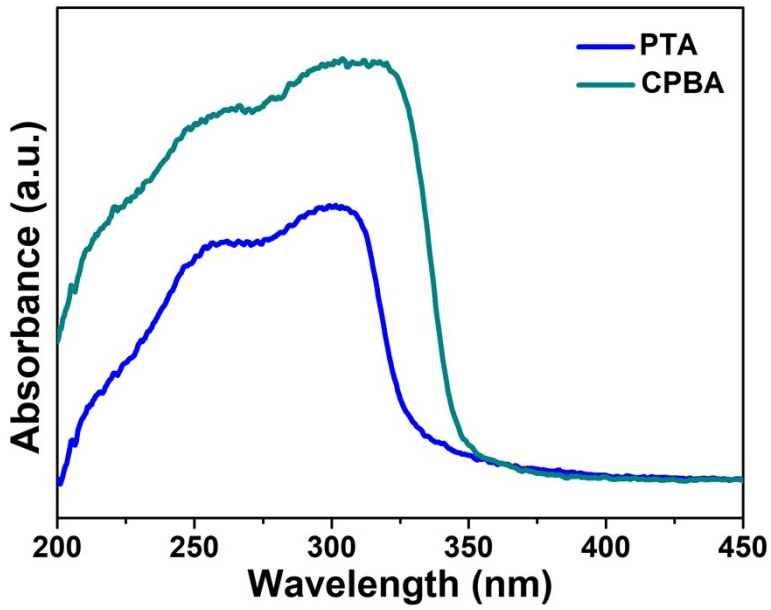

Fig. S23 UV-vis DRS of CPBA and PTA ligand.

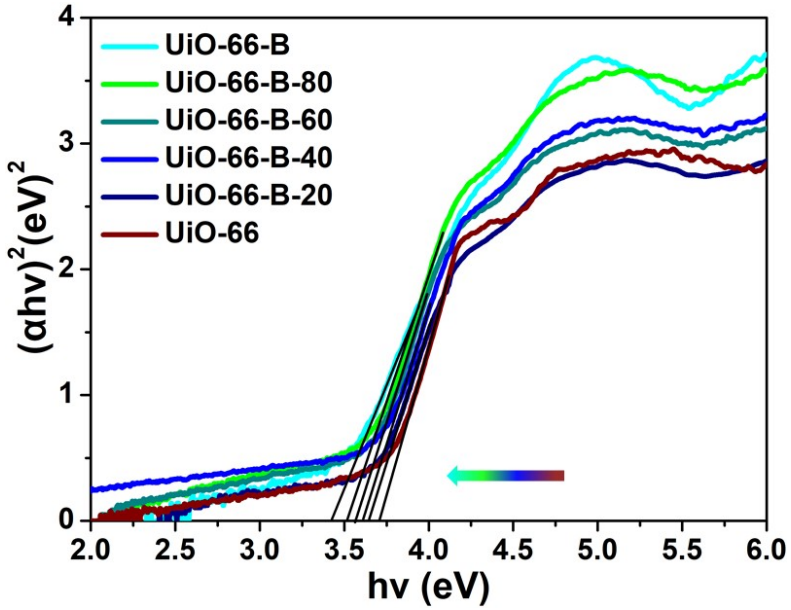

Fig. S24 Tauc plots for direct transition of UiO-66, UiO-66-B-X (X=20, 40, 60, and 80) and UiO-66-B.

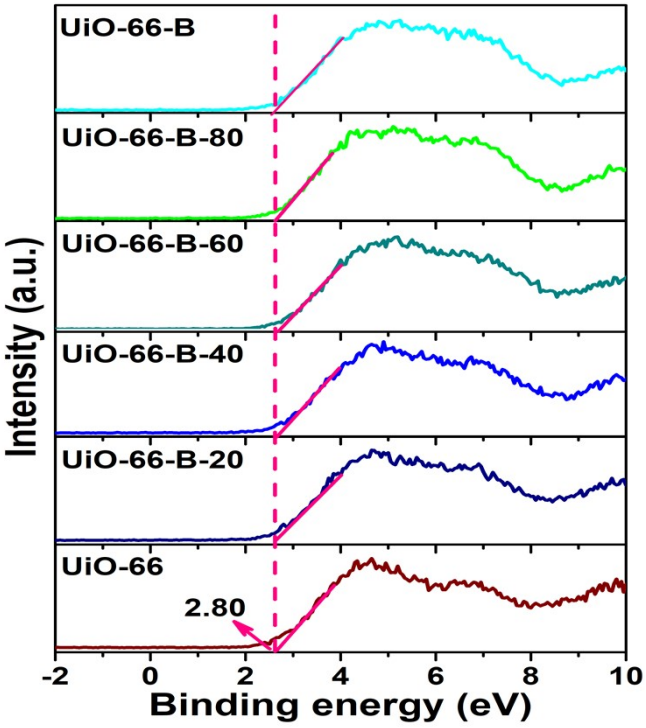

Fig. S25 XPS valence band spectra of UiO-66, UiO-66-B-X (X=20, 40, 60, and 80) and UiO-66-B.

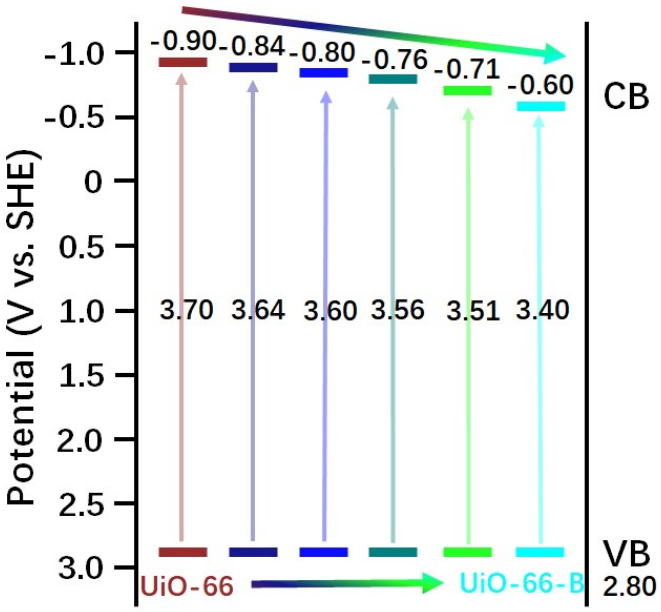

Fig. S26 The estimated band structure of UiO-66, UiO-66-B-X (X=20, 40, 60, and 80) and UiO-66-B.

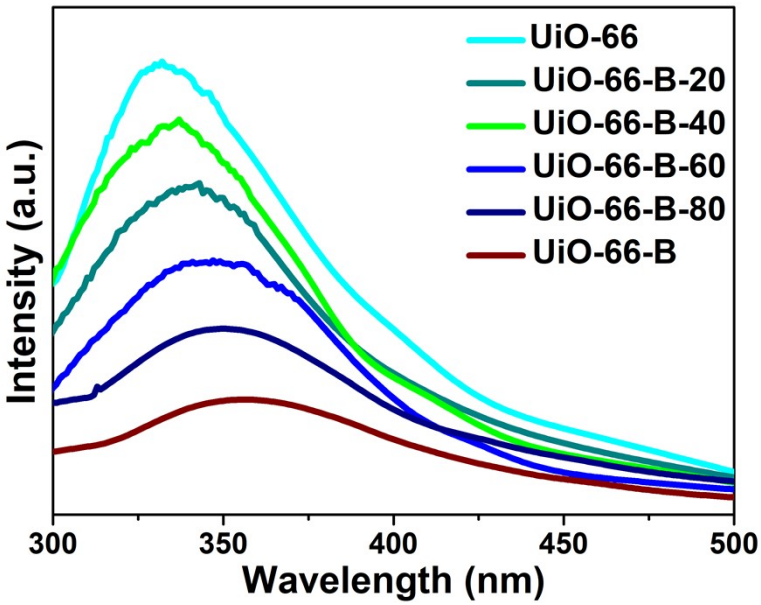

Fig. S27 PL spectra of UiO-66, UiO-66-B-X (X=20, 40, 60, and 80) and UiO-66-B with an excitation wavelength of 280 nm.

Table S1. BET surface area, pore volume and pore size based on N_2 sorption results for UiO-66, UiO-66-B-X (X = 20, 40, 60, 80) and UiO-66-B.

Sample	**BET surface area** ($m^2\ g^{-1}$)	**Pore volume** ($cm^3\ g^{-1}$)	**Pore size** (nm)
UiO-66	956	0.546	2.28
UiO-66-B-20	901	0.497	2.21
UiO-66-B-40	952	0.573	2.41
UiO-66-B-60	934	0.579	2.48
UiO-66-B-80	957	0.469	1.96
UiO-66-B	905	0.489	2.16

Table S2. The comparison for H_2O_2 production with the other reported photocatalysts.

Photocatalyst	Reaction solution	Dosage (mg/mL)	Light source	H_2O_2 (μM g^{-1} h^{-1})	Reference
UiO-66	isopropanol + water	0.3	AM 1.5	314	this work
UiO-66-B	isopropanol + water	0.3	AM 1.5	1002	this work
NH_2-MIL-125(TiO_2)/Ti_3C_2	isopropanol + water	1	λ ≥ 420 nm	280	[1]
Au/TiO_2	ethanol + water	40	λ ≥ 420 nm	13	[2]
SN-GQD/TiO_2	isopropanol + water	0.5	λ ≥ 420 nm	110	[3]
BP-C_3N_4	isopropanol + water	1.7	λ ≥ 420 nm	420	[4]
C_3N_4	isopropanol + water	0.5	AM 1.5	82	[5]
Pt/C_3N_4	isopropanol + water	0.5	AM 1.5	103	[5]
K, P, O-doped g-C_3N_4	ethanol + water	0.5	λ ≥ 420 nm	486	[6]
CdS-graphene	methanol + water	1	AM 1.5	11	[7]
Au/MoS_2	-----	1	real sunlight	132	[8]
Au/$BiVO_4$	pure water	1.7	λ ≥ 420 nm	80	[9]
B doped defected g-C_3N_4	isopropanol + water	0.5	λ ≥ 420 nm	574	[10]

Table S3. Fitted TRPL decay parameters of UiO-66 and UiO-66-B under Ar atmosphere.

Samples	τ_1/ns	B_1	τ_2/ns	B_2	$\tau_{average}$/ns
UiO-66	1.6562	0.118	6.0413	0.029	3.72
UiO-66-B	0.6730	0.182	2.5782	0.030	1.41

Table S4. Fitted TRPL decay parameters of UiO-66 and UiO-66-B under O_2 atmosphere.

Samples	τ_1/ns	B_1	τ_2/ns	B_2	$\tau_{average}$/ns
UiO-66	0.8851	0.080	2.7993	0.015	1.60
UiO-66-B	0.0316	0.962	0.7106	0.040	0.36

References

[1] Y. Wu, X. Li, Q. Yang, D. Wang, F. Yao, J. Cao, Z. Chen, X. Huang, Y. Yang, X. Li, *Chem. Eng. J.* **2020**, *390*, 124519.

[2] Y. Shiraishi, S. Kanazawa, Y. Sugano, D. Tsukamoto, H. Sakamoto, S. Ichikawa, T. Hirai, *ACS Catal.* **2014**, *4*, 774-780.

[3] L. Zheng, H. Su, J. Zhang, L. S. Walekar, H. V. Molamahmood, B. Zhou, M. Long, Y. H. Hu, *Appl. Catal. B* **2018**, *239*, 475.

[4] Y. Zheng, Z. Yu, H. Ou, A. M. Asiri, Y. Chen, X. Wang, *Adv. Funct. Mater.* **2018**, *28*, 1705407.

[5] H. I. Kim, Y. Choi, S. Hu, W. Choi, J. H. Kim, *Appl. Catal. B* **2018**, *229*, 121-129.

[6] G.-H. Moon, M. Fujitsuka, S. Kim, T. Majima, X. Wang, W. Choi, *ACS Catal.* **2017**, *7*, 2886.

[7] S. Thakur, T. Kshetri, N. H. Kim, J. H. Lee, *J. catal.* **2017**, *345*, 78.

[8] H. Song, L. Wei, C. Chen, C. Wen, F. Han, *J. Catal.* **2019**, *376*, 198.

[9] H. Hirakawa, S. Shiota, Y. Shiraishi, H. Sakamoto, S. Ichikawa, T. Hirai, *ACS Catal.* **2016**, *6*, 4976−4982.

[10] C. Feng, L. Tang, Y. Deng, J. Wang, J. Luo, Y. Liu, X. Ouyang, H. Yang, J. Yu, J. Wang, *Adv. Funct. Mater.* **2020**, *30*, 2001922.